Mechanism of Inhibition of SARS-CoV-2 M^{pro} by N3 Peptidyl Michael Acceptor Explained by QM/MM Simulations and Design of New Derivatives with Tunable Chemical Reactivity

Kemel Arafet,[1] Natalia Serrano-Aparicio,[1] Alessio Lodola,[2] Adrian J. Mulholland,[3] Florenci V. González,[4] Katarzyna Świderek,[1,*] Vicent Moliner.[1,*]

1. Departament de Química Física i Analítica, Universitat Jaume I, 12071 Castelló, Spain.
2. Dipartimento di Scienze degli Alimenti e del Farmaco, Università degli Studi di Parma, Italy.
3. Centre for Computational Chemistry, School of Chemistry, University of Bristol, United Kingdom
4. Departament de Química Inorgànica i Orgànica, Universitat Jaume I, 12071 Castelló, Spain.

Keywords: SARS-CoV-2 M^{pro}, COVID-19, inhibition, peptidyl-nitro alkenes, Michael acceptor inhibitors, QM/MM, MD.

ABSTRACT

The SARS-CoV-2 main protease (M^{pro}) is essential for replication of the virus responsible for the COVID-19 pandemic, and one of the main targets for drug design. Here, we simulate the inhibition process of SARS-CoV-2 M^{pro} with a known Michael acceptor (peptidyl) inhibitor, N3. The free energy landscape for the mechanism of the formation of the covalent enzyme-inhibitor product is computed with QM/MM molecular dynamics methods. The simulations show a two-step mechanism, and give structures and calculated barriers in good agreement with experiment. Using these results and information from our previous investigation on the proteolysis reaction of SARS-CoV-2 M^{pro}, we design two new, synthetically accessible N3-analogues as potential inhibitors, in which the recognition and warhead motifs are modified. QM/MM modelling of the mechanism of inhibition of M^{pro} by these novel compounds indicates that both may be promising candidates as drug leads against COVID-19, one as an irreversible inhibitor and one as a potential reversible inhibitor.

INTRODUCTION

A novel coronavirus (severe acute respiratory syndrome coronavirus-2 – SARS-CoV-2) has been identified as responsible for the COVID-19 pandemic. There is a pressing need for effective antiviral treatments. Many researchers around the world are working to develop SARS-CoV-2 antiviral compounds, e.g. following previous SARS-CoV and MERS-CoV outbreaks and research. Remarkable progress has been achieved in just a few months with regard to the understanding of the phylogeny and genomic organization of SARS-CoV-2 as well as its molecular mechanisms of infection and replication.[1] Knowledge of the life cycle of SARS-CoV-2 provides information about possible targets for drug development.[2] These include inhibition of the viral-host interaction, endosome maturation, viral/endosome membrane fusion, and viral polypeptide maturation.[3] Intense work has focused on identification and testing of compounds already approved for the treatment of other diseases such as remdesivir, a pre-existing drug developed against Ebola virus (EBOV),[4] dexamethasone and antimalarial drugs[5]. While some studies show promise, there is a need for new compounds, specific to SARS-CoV-2, both as drug leads and as biochemical probes.[6-9]

The present study is focused on the atomistic characterization of the inhibition mechanism of one of the proteins responsible for the virus replication and maturation, the main coronavirus protease (SARS-CoV-2 M^{pro}, also called $3CL^{pro}$). M^{pro}, together with the papain-like protease PL^{pro}, are cysteine protease (CPs) that process the polyproteins that are translated from the viral RNA in the replication of the SARS-CoV-2 virus. Thus, inhibiting activity of these enzymes would block the viral life cycle. In addition, a distinguishing feature of SARS-CoV-2 M^{pro} with respect to human proteases is its ability to cleave proteins after glutamine residue. This feature, which is shared also by SARS-CoV 3CL protease,[10] has prompted a search for inhibitors incorporating a glutamine residue/mimic in their structure (see below) with the aim of obtaining selectivity in addition to potency.[5] The current scenario explains the recent efforts devoted to the identification of inhibitors of this enzyme, aided by X-ray crystallography,[5, 11, 12] and computational modelling approaches. An example is the Covid Moonshot initiative, which thanks to the contributions of scientists operating all over the world, has identified several potential M^{pro} inhibitors hits which are now under biochemical evaluation.[13]

The best characterized M^{pro} inhibitors so far act with a covalent mechanism. They share a similar recognition moiety, i.e. a peptidomimetic scaffold of moderate size with a glutamine or an isostere at the P1 position and a branched lipophilic group at P2,[5, 11, 12] and are equipped with a reactive ‘warhead’, i.e. an electrophilic group responsible for the covalent

modification of the M^{pro} (see Scheme 1). Warheads so far employed ranged from classical Michael acceptors (MAs) to activated carbonyl derivatives, including alpha-ketoamides and aldehydes.

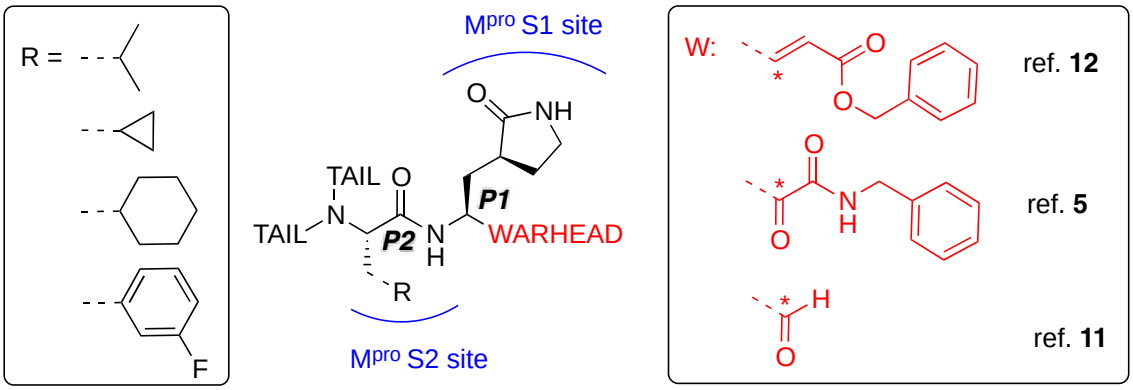

Scheme 1. Schematic representation of the main classes of covalent inhibitors of CoVs M^{pro} so far reported. The reactive center on the warhead is marked with an asterisk. R emerging from P2 residue represents a lipophilic group of moderate size. The tail region is a highly variable portion in term of size and shape and involved other M^{pro} sub-pockets (i.e. S3 and S4) not represented in the scheme.

For covalent modification of cysteine residues, the MA class is often the first choice with several examples of approved drugs containing this group.[14-17] Despite the potential problem of off-target interaction due to the electrophilicity of α,β unsaturated systems, MAs are widely employed against cysteine proteases as they ensure the covalent inhibition of the enzyme.[18] Compounds equipped with less reactive warheads (i.e. carbonyl-based compounds or nitriles) act as reversible inhibitors, as they form metastable adducts (such as hemithioketal or thioimidate species) with cysteine residues. In terms of target engagement, duration of inhibition and efficacy, MAs have key advantages over other warheads.[16-18] Previous work on other viral M^{pro}s exemplifies this: peptidyl MAs were the first class of mechanism-based covalent inhibitors of CoV M^{pro} enzymes described in 2005.[19] This seminal work prompted Jin and colleagues[12] to test this library of compounds on the SARS-CoV-2 M^{pro}. Among those compounds, they found that one of them, **N3** (see Scheme 2), shows promising inhibitory activity against the M^{pro} of SARS-CoV-2.

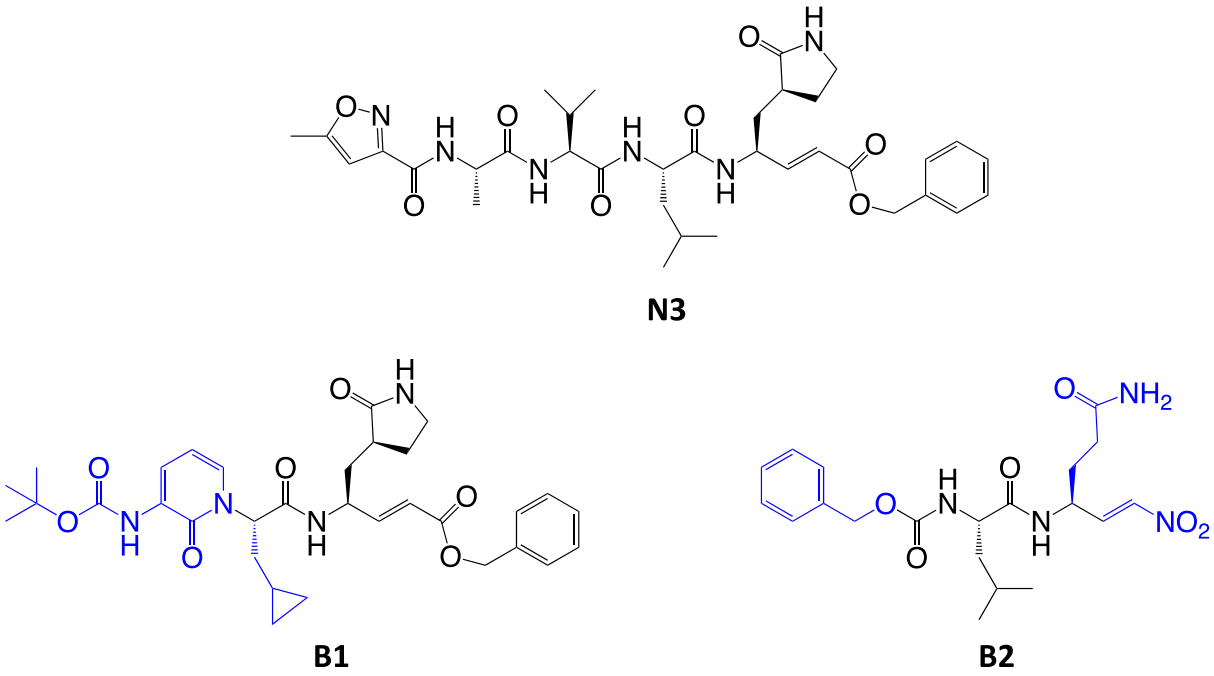

Scheme 2. Chemical structures of known (N3) and proposed (B1 and B2) Michael acceptor inhibitors of SARS-CoV-2 M^{pro}. The modifications from **N3** to **B1** and **B2** are highlighted in blue.

Kinetic analysis of the inhibition of M^{pro} of SARS-CoV-2 by N3 suggests a mechanism of two steps leading to irreversible inactivation (see Scheme 3): protein-inhibitor association to form a noncovalent complex (**E:I**), followed by covalent bond formation (**E-I**).[5] The X-ray diffraction structure showed a covalent bond between the S atom of Cys145 of protomer A and the Cβ atom of the vinyl group (see Scheme 3), thus confirming that **N3** is a MA inhibitor[12] and confirming that SARS-CoV-2 M^{pro} is a CP with an active site catalytic dyad (C145/H41) similar to other CPs.

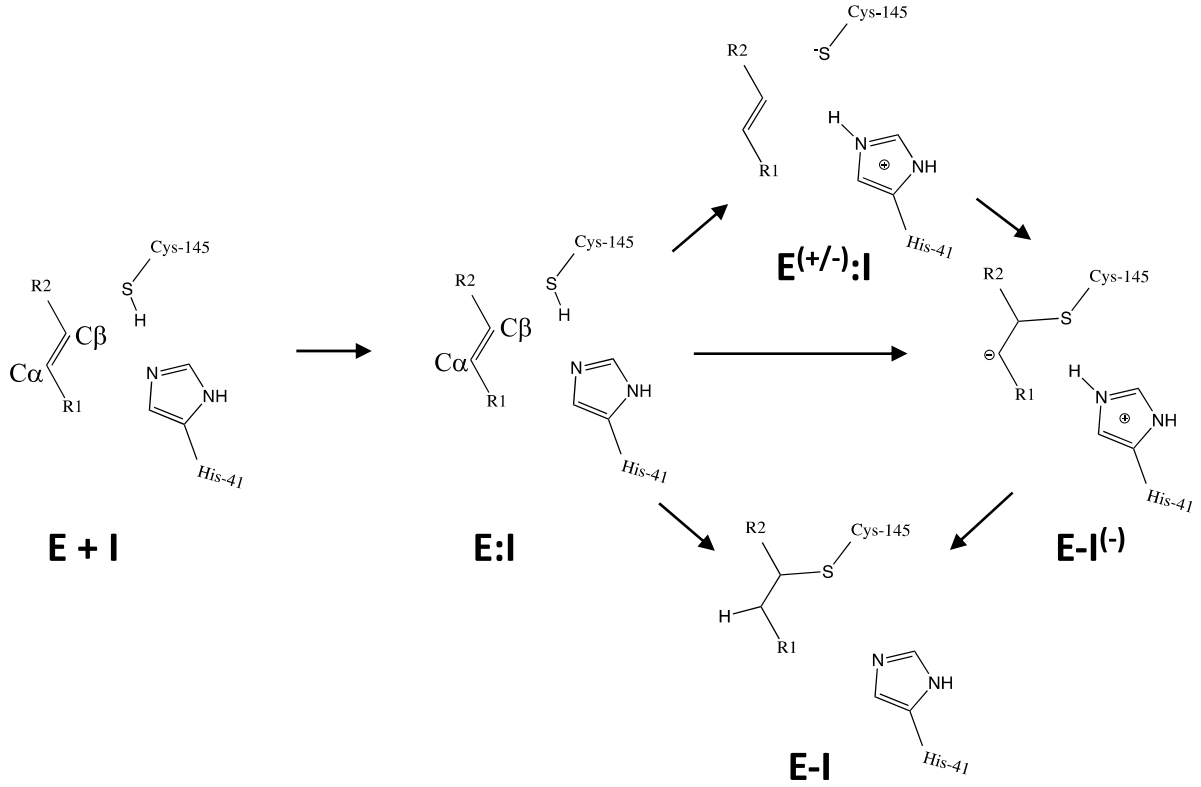

Scheme 3. Proposed general mechanisms of SARS-CoV-2 M^{pro} cysteine protease inhibition by Michael acceptor inhibitors: concerted or stepwise Michael addition. R1 and R2 represent different substituents, as shown in compounds depicted in Scheme 2.

Crystallographic electron density maps of **N3**[12] indicate hydrogen bond and van der Waals interactions between the inhibitor and residues in the substrate-binding pockets of M^{pro}. An exception is the solvent-exposed Val at P3, suggesting that this site can tolerate substituents of different shape and size.[12]

Mechanistically, it is proposed that the chemical reaction leading to M^{pro} inactivation requires the imidazole group of H41 to activate the SH group of C145 to form a highly nucleophilic $CysS^-/HisH^+$ ion pair that would readily react with the inhibitor.[20] This equilibrium may be tipped in favour of the ion pair by ligand binding, and may depend on the features of the ligand itself. In this regard, the inactivation of SARS-CoV-2 M^{pro} by covalent (peptidyl) inhibitors, including **N3**, can be considered as equivalent to the acylation step of the proteolysis reaction in CPs. According to our previous QM/MM study on the proteolysis reaction catalyzed by cruzain CP, the proton from the cationic $HisH^+$ is transferred to the N atom of the scissile peptide bond, followed by Cys attack on the carbonyl carbon atom of the peptide.[21] However, our recent study on the proteolysis reaction of SARS-CoV-2 M^{pro} using as substrate the polypeptide Ac-Val-Lys-Leu-Gln-ACC (ACC being a fluorescent tag 7-

amino-4-carbamoylmethylcoumarin) suggests that the mechanism of action of this enzyme slightly differs from other cysteine proteases.[22] First of all, the enzyme:substrate initial complex would correspond to the neutral C145/H41 dyad (equivalent to **E:I** in Scheme 3) instead of the ionic pair dyad $C145^{-}/H41^{+}$ ($\mathbf{E^{(+/-)}:I}$ in Scheme 3). From this stable state, the acylation reaction consists of a proton transfer from C145 to the H41 concomitant with the nucleophilic attack on the carbonyl carbon atom of the peptide bond by the sulfur atom of C145, leading to a pseudo-stable intermediate. Then, the cleavage of the peptide bond by M^{pro} is assisted by proton transfer from the protonated $H41^{+}$ to the nitrogen atom of the substrate, forming an acyl-enzyme covalent intermediate. This last step of the acylation was calculated to be almost barrierless with the substrate employed in our previous study.[22] In the inhibition reaction by MA compounds shown in Scheme 2, the proton will be transferred from the protonated $H41^{+}$ to the Cα of the inhibitor, thus leading to the covalent **E-I** adduct (Scheme 3). Consequently, in the design of covalent inhibitors, focus must be put on obtaining an exergonic process for the **E-I** formation, with low activation energy barriers. The energy barriers from **E-I** back to reactants **E:I** will determine the irreversible vs reversible character of the inhibitors, with potentially paramount importance for finding the optimal balance between efficacy and safety. To reach this goal, in addition to the presence of a reactive warhead, the interactions between the recognition moiety of the inhibitor and the different sub-sites of the binding pocket of the protein must be taken into account, which can be guided by the results derived from previous studies on this and related CPs. QM/MM simulations provide a good tool to investigate the reactivity of covalent inhibitors within their protein targets.[23-29]

Here, we focus firstly on the inhibition of the SARS-CoV-2 M^{pro} by the covalent (peptidyl) irreversible inhibitor **N3,** modelling the reaction with QM/MM techniques. Building upon the findings, on information derived from other CP inhibitors and on our previous study on the proteolysis reaction of M^{pro},[22] we then designed, and tested computationally, two MA inhibitors to block the enzyme: compounds **B1** and **B2** in Scheme 2. **B1** was designed according to some of the modifications made by Zhang et al.[5] on their broad-spectrum peptidomimetic α-ketoamides inhibiting of the main proteases of betacoronaviruses, alphacoronaviruses and the 3C proteases of enteroviruses.[30] In addition, although the inhibition of CPs is dependent on the interactions between the peptidic framework (the P2) of the inhibitor and the S2 pocket of the enzyme,[28, 31-34] this is probably not the case in SARS-CoV-2 M^{pro}, according to the QM-MM protein-substrate interactions found in our previous study of the proteolysis reaction of SARS-CoV-2M^{pro} [22]: S2 appears to be a small

hydrophobic pocket without strong hydrogen bond interactions. Therefore, the isopropyl group of Leu at P2 site was replaced by a cyclopropyl group. This change is in accordance with the changes by Zhang et al. to the original peptidomimetic α-ketoamides to enhance anti-viral activity against beta coronaviruses (such as SARS-CoV and SARS-CoV-2).[5] The tail of the **N3** compound was replaced by an amino pyridone moiety carbamoylated by a *tert*-butyloxycarbonyl group, because this group is expected not to be a substrate of cellular proteases, and so offers potential advantages in term of pharmacokinetic properties.[5] Our previous M^{pro} proteolysis reaction study indicated that the S3 subsite is completely exposed to the solvent and only three interactions between the peptide backbone atoms of Lys3 of the substrate and the protein were observed.[22] In addition, the lack of possible strong hydrogen bond interactions in S4 sub-site supports the strategy of reducing the size of the inhibitor.

In the case of compound **B2**, a more dramatic modification was introduced: we decided to change the warhead to a nitroalkene, based on the potent reversible inhibitory activity of a family of dipeptidyl nitroalkene derivatives against the CPs cruzain and rhodesain by one of us,[14] together with our previous QM/MM study on the inhibition mechanism of three CPs belonging to the papain family (cruzain, rhodesain, and cathepsin L).[28] Based upon the mechanism depicted in Scheme 3, the protonation of intermediate **E-I**$^{(-)}$ might be less favored in the case of the nitroalkane carbanion arising because the acidity of the corresponding acid, namely the nitroalkane, is higher, and thus, the basicity of the carbanion is lower; potentially the cause of being a covalent reversible inhibitor. The glutamine residue in P1 was introduced due to the strong favorable interactions that we observed in the study of the proteolysis of the Ac-Val-Lys-Leu-Gln-ACC substrate by M^{pro},[22] and based on the substrate specificity of SARS-CoV M^{pro} , i.e. requiring glutamine in the P1 position.[35] P2 was kept the same as in **N3**, while the rest of the inhibitor in positions P3, P4 and P5 was replaced by a smaller moiety, with the aim of improving the physicochemical properties as well as synthetic accessibility. Importantly, both designed compounds **B1** and **B2** should be readily prepared through synthetic approaches inspired by published synthetic routes of similar compounds.[13,36]

COMPUTATIONAL METHODS

The coordinates of atoms of SARS-CoV-2 M^{pro} were taken from the X-Ray structure of its complex with the **N3** inhibitor, available in the Protein Data Bank (PDB ID 6LU7).[12] The biological assembly (homodimer) was built using Discovery Studio Visualizer 19. Inhibitor **N3** was replaced by two Michael acceptor inhibitors (compounds **B1** and **B2**) to create two new covalent enzyme-inhibitor models (**E-I** in Scheme 2). Once the enzyme-inhibitor models were set up, solvated with a box of water molecules and equilibrated by means of preliminary MM molecular dynamics (MD) simulations (Fig. S1a, S2a and S3a), QM/MM free energy surfaces (FESs) were obtained, in terms of Potentials of Mean Force (PMFs), for every step of the reaction using umbrella sampling[37] combined with the Weighted Histogram Analysis Method (WHAM).[38] See Supporting Information for details. The QM region consisted of 75 atoms for the inhibitor **N3** and compound **B1**, and 57 atoms for the compound **B2** including P1', P1 and P2 fragments of the inhibitors and the two catalytic residues C145 and H41. Three quantum 'link' atoms were inserted where the QM-MM frontier crosses a covalent bond (See Fig. S1b, S2b and S3b). The Austin Model 1 (AM1)[39] semiempirical method was used to treat the QM region in the initial exploration of the FESs, while the Minnesota Functional M06-2X[40] with the standard 6-31+G(d,p) basis set,[41] were used to treat the QM region, as implemented in Gaussian09 program,[42] to provide the final corrected high level FESs (see Supporting Information for details). This is a good choice of functional and basis set, based on our previous tests experience,[43-45] including the study of the proteolysis reaction of SARS-CoV-2 M^{pro}.[22] The protein and water molecules were treated with the AMBER ff03[46] and TIP3P[47] force fields, respectively. QM/MM MD simulations were performed using the fDynamo library,[48] using procedures that we have previously extensively tested and validated. Structures of all the states involved in the reaction (minima and transition state structures) were optimized at M06-2X:6-31+G(d,p)/MM level, starting from representative AM1/MM snapshots of the FESs with Gaussian09 program[42] coupled to fDynamo library. These are deposited in the Supporting Information.

The estimation of the inhibitor:M^{pro} binding energy was performed by docking calculations for **N3**, **B1** and **B2,** with the Glide program,[49] starting from the QM/MM structures of the enzyme:inhibitor non-covalent reactant complex, **E:I** in Scheme 2 (see Supporting Information for details).

RESULTS AND DISCUSSION

Inhibition reaction of SARS-CoV-2 M^{pro} with N3. The first step of our program towards the rational design of new SARS-CoV M^{pro} inhibitors was the study of the reaction with the **N3** inhibitor originally proposed by Yang et al.[19] As described in the Methods section, the enzyme-inhibitor covalent **E-I** complex was equilibrated by MM and QM/MM MD simulations. A schematic representation of the equilibrated structure of the active site is shown in Fig. 1, where important interactions found in the MD simulations and the X-ray structure obtained by Jin et al.[12] are indicated as blue and red dashed lines, respectively. The pattern of interactions between the enzyme and the inhibitor in our equilibrated structure is quite close to that observed experimentally, thus supporting our starting structure for the exploration of the full mechanism. The MD results confirm the absence of hydrogen bond interactions with some of the side chains of the residues of **N3** (P2-P5) which, considering the demonstrated efficiency of this inhibitor, can be used as a guide for the design of improved compounds not requiring hydrogen bond interactions with these sites, as mentioned in the Introduction.

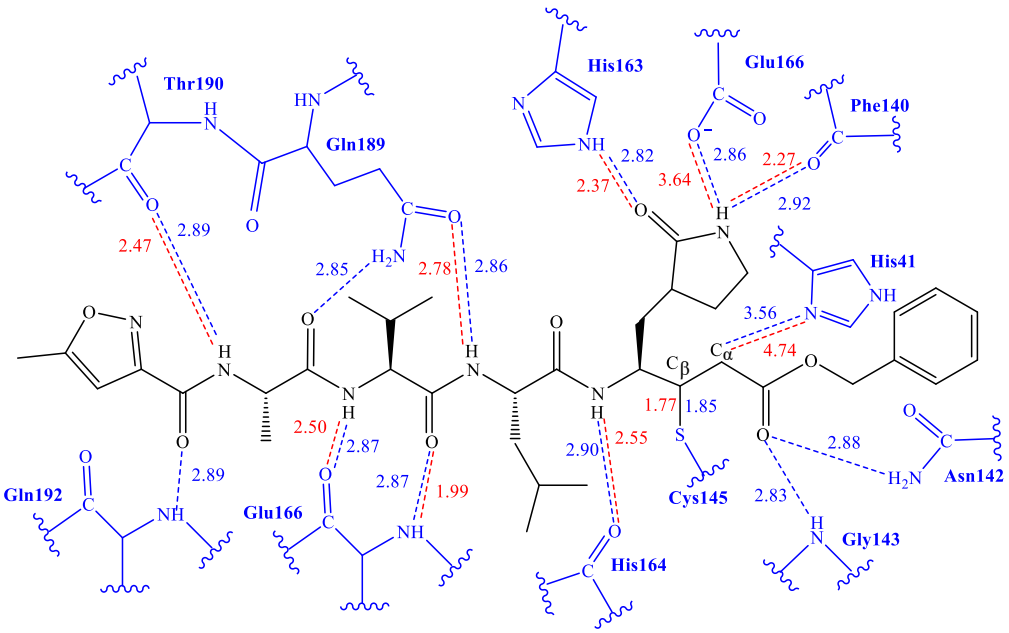

Figure 1. Schematic representation of **N3** in the covalent **E-I** complex in the active site of SARS-CoV-2 M^{pro}. The dashed lines indicate hydrogen bond interactions between the inhibitor the protein deduced from MD simulations (blue lines) and the X-ray structure (red lines) obtained by Jin et al.[12] Distances are reported in Å.

Once the covalent enzyme-inhibitor **E-I** complex was equilibrated, the Michael addition reaction and the proton transfer from the protonated H41 to the Cα atom of the inhibitor (see

Scheme 3) was explored backwards from **E-I** to **E:I** by QM/MM MD simulations. Different combinations of interatomic distances were employed to generate the potential energy surfaces (PESs) and the free energy surfaces (FESs) of every chemical step. The FESs obtained (see Fig. S4 in Supporting Information) show that the more stable protonation state of the C145/H41 dyad corresponds to that in which both residues are neutral, designated **E:I**. This result is in contrast with previous computational studies of proteolysis[21] and inhibition[24, 28, 50] of other CPs, but it is in agreement with our previous study of the proteolysis reaction of M^{pro},[22] and previous work suggesting substrate binding induced ion pair formation in other SARS-CoV Main proteases.[51] From this initial state, the proton transfer from C145 to H41 to form the ionic dyad $\mathbf{E^{(+/-)}:I}$ precedes the Michael addition that forms the covalent bond between the sulphur atom of C145 and the Cβ of the inhibitor, to form $\mathbf{E:I^{(-)}}$. Finally, the proton transfer from His41 to Cα of the substrate takes place as an almost barrierless process to produce the final, stable, **E-I** covalent complex. The resulting free energy profile is shown in Fig. 2, and details of the active site in the key states in the inhibition process are presented in Fig. 3. The reaction is a stepwise process, kinetically controlled by the carbon-sulphur bond formation, via TS2, with a free energy barrier of 11.2 kcal·mol^{-1}, and a reaction energy of –17.9 kcal·mol^{-1}. The low activation free energy of the inhibition reaction with **N3** is in agreement with the experiments that revealed a process so fast that the enzyme inactivation-rate constant for covalent bond formation could not be measured.[12] Regarding the thermodynamics, the resulting energy profile is in agreement with the irreversible character of the inhibition considering that activation barrier for the reverse retro-Michael reaction is nearly 30 kcal mol^{-1} (computed as the difference between **E-I** and **TS2**). On the other side, the free energy of activation for the initial proton transfer from C145 to H41 is very low (1.4 kcal·mol^{-1}) and the relative energy of the ion pair dyad, $\mathbf{E^{(+/-)}:I}$, is only 1.3 kcal·mol^{-1} higher than the starting **E:I** state (see red line in Fig. 2a). It is important to point out that while preparing the present manuscript, a QM/MM MD study on the mechanism of **N3** has appeared.[52] Comparison of the two studies reveals some analogies but also some important differences. The stepwise and the exergonic character of the reaction, and the finding that the neutral **E:I** form is more stable than the ion pair $\mathbf{E^{(+/-)}:I}$, are common to both studies. However, while our $\mathbf{E^{(+/-)}:I}$ is just 1.3 kcal·mol^{-1} higher in energy than **E:I**, the difference obtained in the other study is much higher (10.3 kcal·mol^{-1}). Similarly, they found a much higher energy barrier for the C145 - Cβ bond formation from **E:I** (20.9 kcal·mol^{-1}). The mechanism is also slightly different because a water molecule is used in the transfer of the

proton from His41 to Cα of the inhibitor while, as commented above, our simulations show that the direct transfer can take place, in an almost barrierless process, as previously for other CP inhibition reactions by Michael acceptors.[28, 50] We note that, all other things being equal, the lower barrier found here (not involving an intervening water molecule), indicates that the mechanism we find would dominate the experimentally observed kinetics.

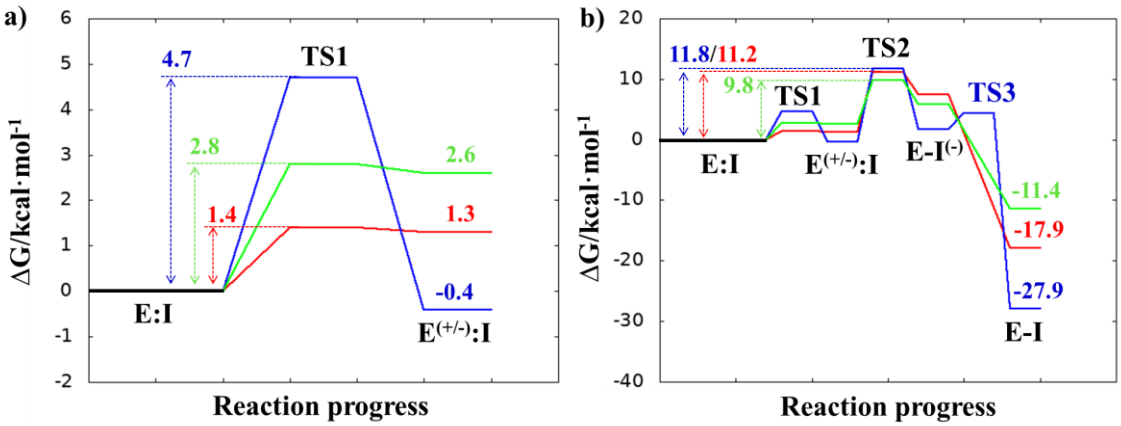

Figure 2. M06-2X/6-31+G(d,p):AM1/MM free energy profiles for covalent complex formation with SARS-CoV-2 M^{pro} and: **N3** (red line); compound **B1** (blue line); and compound **B2** (green line). Panel (a) shows the formation of the ion pair **E$^{(+/-)}$:I**; and the full inhibition reaction is shown in panel (b). Energies are in kcal·mol^{-1}.

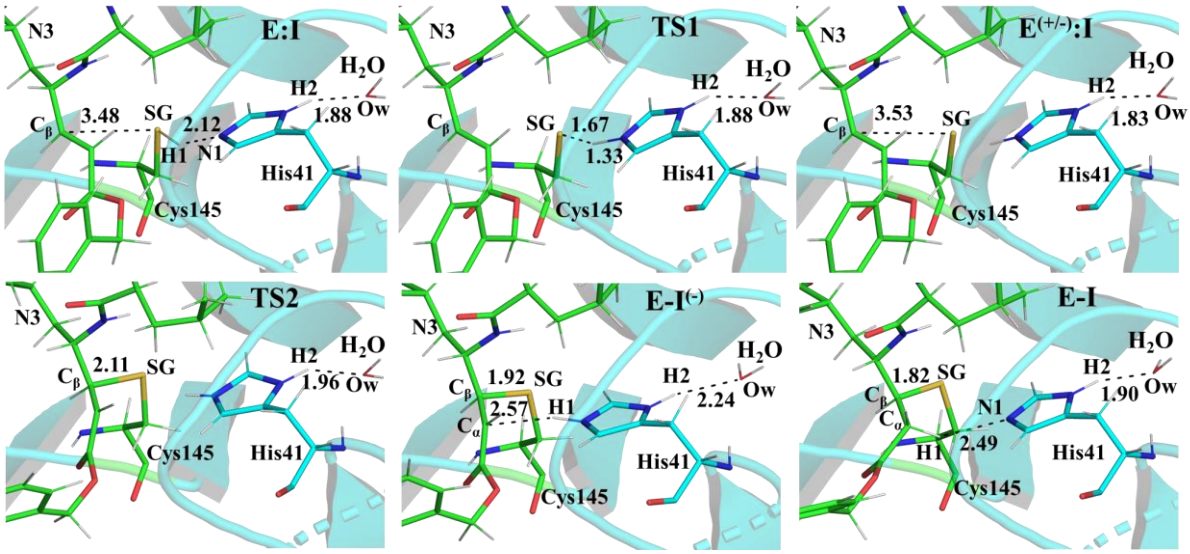

Figure 3. M06-2X/6-31+G(d,p)/MM optimized structures of the important states in the inhibition process of M^{pro} by **N3**. Distances are shown in Å.

Analysis of the structures of the key states in the reaction (Fig. 3, Table S4 and S5) confirms the mechanism and suggests that the active site of the M^{pro} does not undergo dramatic changes during the chemical steps. The two catalytic residues are well oriented in the reactive non-covalent complex **E:I** in which the inhibitor is well anchored to the active site. Structures of

TS1 and TS2 were optimized at M06-2X/6-31+G(d,p)/MM level and the minimum energy path, computed as the IRC path, confirms the predictions derived from the M06-2X:AM1/MM FESs (see Table S4, S5 and S6).

In order to analyse the non-covalent enzyme:inhibitor reactant complexes, **E:I**, the interaction energies (electrostatic plus Lennard-Jones) between residues of Chain-A of M^{pro} and each fragment of the **N3** were computed as an average over 1000 structures of the equilibration AM1/MM MD simulation (Fig. 4). The pattern of interactions is similar to that of **E-I**, shown in Fig. 1, confirming that the inhibitor and enzyme undergo no large structural changes during the chemical steps of the inhibition process. It is important to point out that, while there are protein residues that clearly bind the inhibitor in the active site, which could have been predicted by the X-ray geometrical analysis of the **E-I** complex (N142 and G143 in P1':::S1', H163, E166, F140 and H164 in P1:::S1, Q189 in P2:::S2, E166 in P3:::S3, T190 in P4:::S4 or Q192 in P5:::S5), some of these residues do not form binding interactions in **E:I**. For instance, interatomic distances (Table S4), suggest that E166 forms a hydrogen bond with the backbone of P3, but no net stabilizing interaction was measurable (Fig. 4 and Fig. S5) in **E:I**. Therefore, design of **N3** analogues to generate a more stable enzyme-inhibitor initial complex should not be limited to geometrical analysis of X-ray structures or those derived from MD simulations of the reactant complex. Overall, our results suggest that P1 is the most important fragment to consider in the design of new efficient inhibitors. This accords with the conclusions of our previous QM/MM study of the proteolysis reaction of M^{pro}.[22]

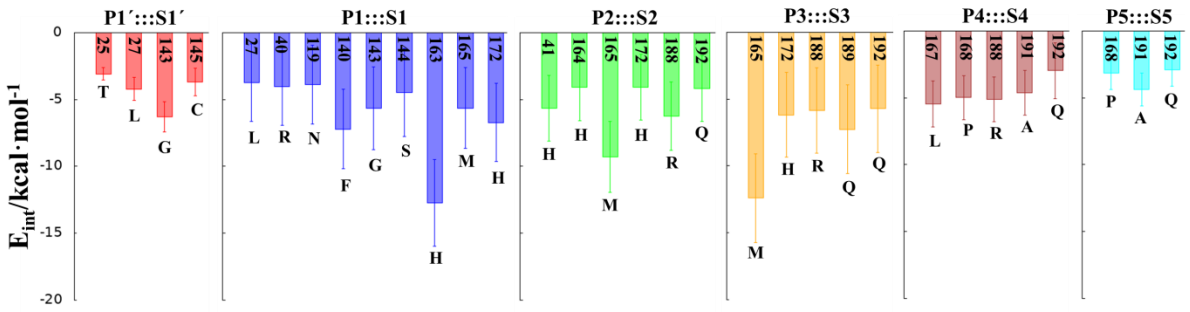

Figure 4. Main favorable average interaction energies (electrostatic plus Lennard-Jones) between residues of Chain-A and each fragment of the **N3** computed in the **E:I** state. Results obtained as an average over 1000 structures of the AM1/MM MD simulations.

Designed Inhibitors of SARS-CoV-2 M^{pro}: compounds B1 and B2. After the study of the Michael addition with inhibitor **N3**, the inhibition reactions of M^{pro} with compounds **B1** and **B2** were simulated following the same methods. The calculations analyzed the stability of the

E-I complexes, with special attention to the protein-inhibitor interactions. A schematic representation of the equilibrated **E-I** structures of the active site after the QM/MM MD simulation is shown in Fig. 5. The interactions between the enzyme and the two proposed inhibitors, indicated as dashed blue lines in Fig. 5, confirm the predictions of the design. In both cases, the interactions between the protein and the inhibitor are dominated by the P1':::S1' and the P1:::S1. Apart from these interactions, in the case of compound **B1**, hydrogen bond interactions in P4 (with Gln192) are found, while in the case of compound **B2** more strong interactions appear, especially in P3 (with Glu166). These interactions keep both compounds posed appropriately for covalent bond formation to take place.

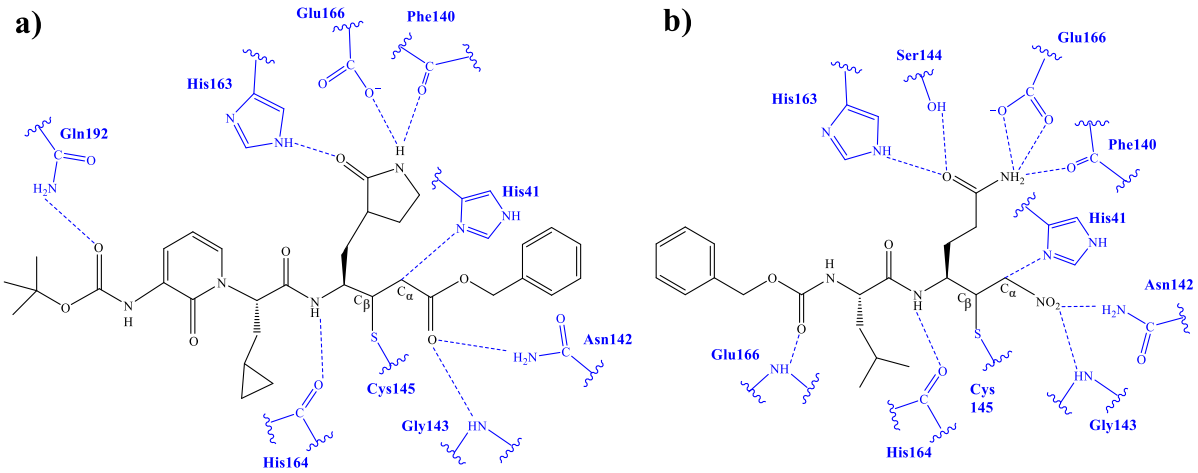

Figure 5. Schematic representation of the active site in the **E-I** complex and detail of the H-bond interactions between the inhibitor and the active site of SARS-CoV-2 M^{pro} as derived from QM/MM MD simulations of compound **B1** (a) and compound **B2** (b).

After equilibration of the two covalent **E-I** structures, the chemical reaction steps of the (reverse) inhibition process were studied by exploration of the PESs and FESs (Fig. S6 and S8). The free energy profiles are shown in Fig. 2, together with that for **N3**. The reaction in both cases follows the same mechanism as for **N3**. The activation energy barriers obtained with compound **B1** and **B2**, are both determined by the rate-limiting transition state of the C-S bond formation, TS2. Nevertheless, while the barrier (for covalent complex formation, i.e. for the forward reaction) of **B1** (11.8 kcal·mol^{-1}) is very close to that obtained with **N3** (11.2 kcal·mol^{-1}), that of B2 is slightly lower (9.8 kcal·mol^{-1}). In contrast, the reaction energies of **B1** and **B2** are very different: –27.9 and –11.4 kcal·mol^{-1}, respectively. These results suggest, first, that both designed inhibitors should present similar reactivity to **N3** for covalent complex formation, **B2** being slightly more reactive. Second, while compound **B1** would be an irreversible inhibitor, compound **B2** is predicted to be more reversible inhibitor character than **B1** and **N3**. As can be seen from Fig. 2a, there are also differences regarding the relative

energy of the initial non-covalent states, **E:I** vs **E$^{(+/-)}$:I**. While in the case of compound **B1** the neutral dyad is 0.4 kcal·mol^{-1} less stable than the ionic pair, the **E$^{(+/-)}$:I** of compound **B2** is 2.6 kcal·mol^{-1} higher in energy than the **E:I**. As observed in Fig. 2a, **E$^{(+/-)}$:I** of compound **N3** is also higher in energy, by 1.3 kcal·mol^{-1}, than the **E:I**. These results, compared with the results obtained with **N3**, with the previously studied proteolysis reaction with a reactive substrate,[22] and with previous studied on other SARS-CoV M^{pro} enzymes[51] indicate that the protonation state of C145 and H41 in the initial non-covalent binary complex depends on the substrate substituents in the P1', P1 and P2 positions. Thus, it is remarkable how, according to the P1′:::S1' interatomic distances, the interaction established between the nitro group of **B2** and G143 appear to be stronger in the **E:I** than in **E$^{(+/-)}$:I**, in contrast to **B1,** that shows a small diminution in the distances between the carbonyl group and residues G143, or **N3** that does not show any clear trend in the interactions with residues G143, S144 and C145 (see Tables S4, S7 and S10). The different electronic distributions in these moieties of the substrate, a less basic carbanion in **B2** as compared to **N3** and **B1**, can slightly shift the pKa of the two catalytic residues. Nevertheless, as shown in Fig. 2, the influence is not significant for the inhibition process of M^{pro}. Finally, while the final proton transfer from H41 to the Cα of the inhibitor takes place as a barrier less process in **N3** and **B2**, a transition state, **TS3**, has been localized for the reaction with **B1**, despite with a very small energy barrier (2.7 kcal·mol^{-1}).

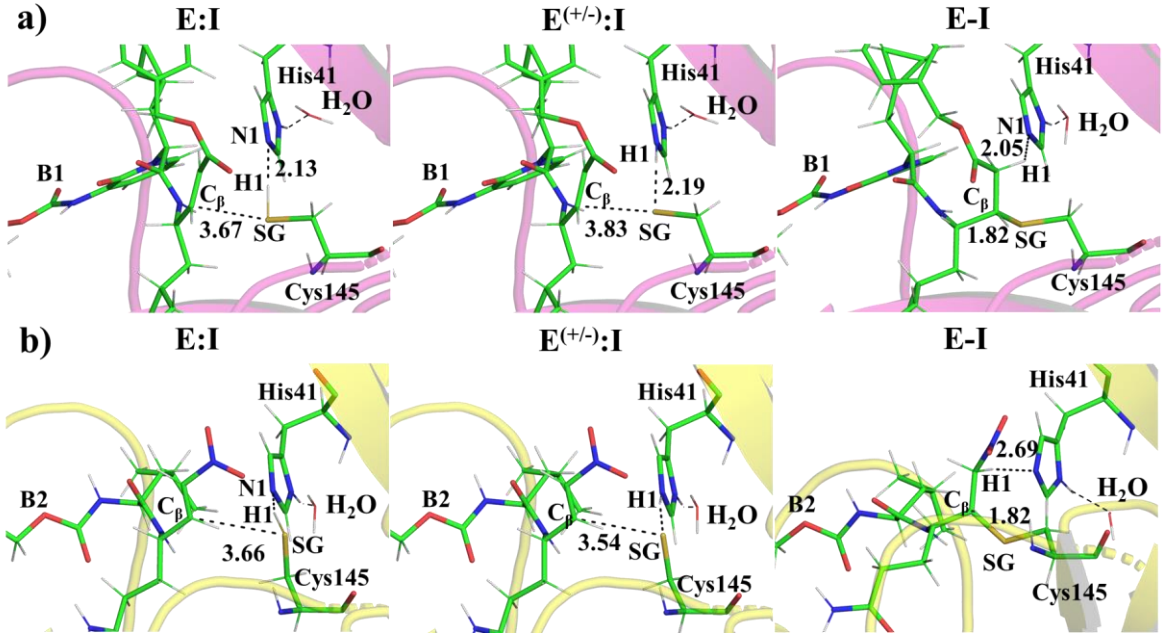

Figure 6. M06-2X/6-31+G(d,p)/MM optimized structures of **E:I**, **E$^{(+/-)}$:I** and **E-I** appearing along the inhibition process of M^{pro} by compound **B1** (a) and compound **B2** (b). Key distances are reported in Å.

M06-2X/6-31+G(d,p)/MM optimized structures of the stable states appearing along the reaction with both inhibitors are presented in Fig. 6 (structures of the TSs, **E:I** and **E-I** are deposited in the Supporting Information together with a list of key interatomic distances of average structures obtained from the AM1/MM MD simulations and single optimized structures at M06-2X/6-31+G(d,p)/MM level). As observed for **N3**, the enzyme-inhibitor interactions do not change during the chemical steps of the inhibition reaction with **B1** and **B2** (Fig. 6 and Tables S7 and S10). In both cases, designed inhibitors bind stably in the active site of the enzyme. Analysis of the favorable protein-inhibitor interactions in the **E:I** state, computed as the sum of QM/MM electrostatic and Lennard-Jones terms, shown in Fig. 7, confirms the predictions assumed during the design of **B1** and **B2** and the conclusions from the geometrical analysis of the optimized structures. In both cases the interactions between the protein and the inhibitors are dominated by those in the P1:::S1 site.

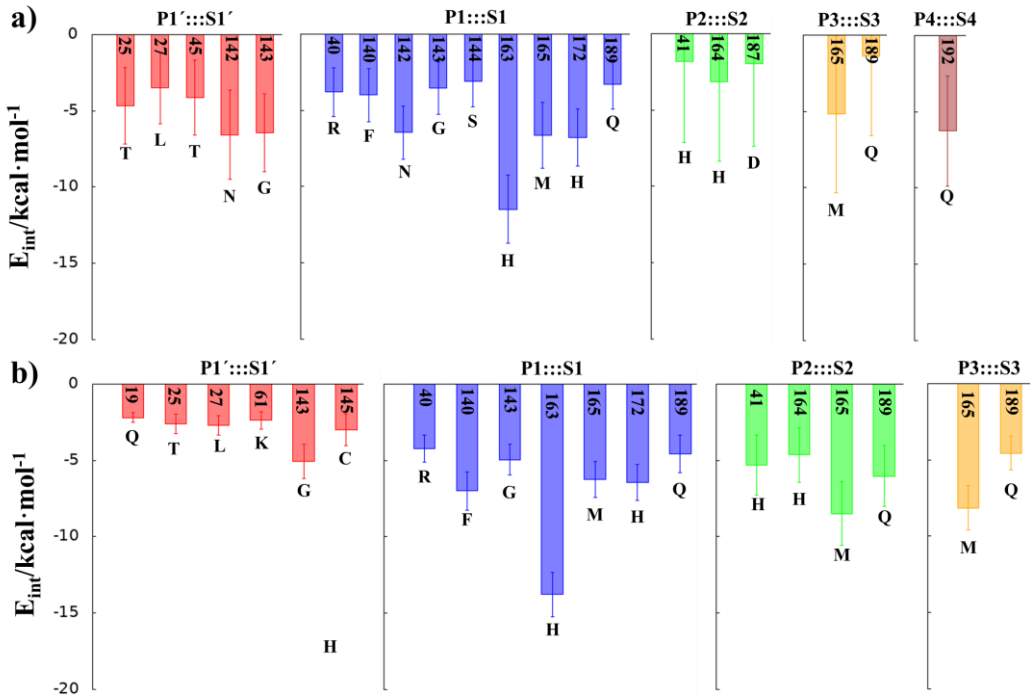

Figure 7. Main favorable average interaction energies (electrostatic plus Lennard-Jones) between residues of Chain-A and each fragment of the compound **B1** (a) and compound **B2** (b) computed in the **E:I** state. Results obtained as an average over 1000 structures of the AM1/MM MD simulations.

The averaged structures of $\mathbf{E^{(+/-)}}$**:I** and **TS2** in the three compounds (Tables S4, S7 and S10), as deduced from the QM/MM MD simulations, show how the change of the reaction coordinate in this rate limiting step (the change in the distance between the SG atom of C145 and the Cβ atom of the inhibitors from $\mathbf{E^{(+/-)}}$**:I** to **TS2**) is larger in the reaction with **N3** and **B1**

(1.06 and 1.20 Å, respectively) than in the reaction with **B2** (0.89 Å). The same conclusion is obtained if comparing the change of this coordinate from the initial **E:I** complex: the smaller the change of the coordinate from **E:I** complex to the **TS2** (1.09, 1.14 and 0.74 Å for **N3**, **B1** and **B2**, respectively), the lower the barrier (11.2, 11.8 and 9.8 kcal·mol^{-1} for **N3**, **B1** and **B2**, respectively). These results suggest that structure of the inhibitors and their interactions with the protein makes that **B2** adopts a more reactive conformation on the **E:I** and **E$^{(+/-)}$:I** states, closer to **TS2** than those in the case of **N3** or **B1**, thus explaining its lower activation energy barrier. These results explains why the inhibitor in which the ion pair is most disfavored, but closer to the rate limiting **TS2**, is also the one with the lowest overall barrier.

Estimation of inhibitor:Mpro binding energy. Binding of inhibitors to M^{pro} active site through noncovalent interactions (to form **E:I**, Scheme 3) is a key event that precedes the chemical step of the inhibitory process. To estimate this binding energy, docking of **N3**, **B1** and **B2** was performed, starting from the structures of the reactants generated by QM/MM MD simulations. Docking indicates that all the inhibitors assume a binding pose consistent with the X-ray structure of the M^{pro}-**N3** adduct, i.e. with the warhead properly oriented to react with the catalytic cysteine, the polar sidechain at P1 site forming hydrogen bonds with S1 residues, and the lipophilic chain at P2 site undertaking several van der Waals contacts with S2 residues (Fig. S10). The reference **N3** inhibitor gave a G_{score} of –14.4 kcal·mol^{-1}, consistent with the high number of hydrophilic and lipophilic contacts formed by this compound within the M^{pro} active site. Compounds **B1** and **B2** are also predicted to bind with good affinity (G_{score} values, –10.6 and –8.6 kcal·mol^{-1}, respectively). The less negative score of these putative inhibitors is due to their smaller size compared to **N3**. The binding poses of **B1** and **B2** resemble that of **N3** (Fig. S10), suggesting that modifications at level of the tail or of the warhead do not affect the accommodation of the critical P1 and P2 residues. Within the known limits of empirical scoring functions, the present docking analysis supports the proposal that **B1** and **B2** can bind to M^{pro} in a productive orientation in its active site.

CONCLUSIONS

Here, we first explored the inhibition of SARS-CoV-2 M^{pro} with a known covalent (peptidyl) inhibitor, **N3**,[19] by QM/MM MD simulations. The results are in good agreement with experimental crystal structures and kinetics, and reveal the chemical mechanism of covalent reaction. This provides an atomically detailed description of the process of formation of the covalent enzyme-inhibitor complex. We used these results, together with information for

other CP protease inhibitors, and from our recent study of the proteolysis reaction of SARS-CoV-2 M^{pro},[22] to design and computationally test two putative inhibitors of SARS-CoV-2 M^{pro} based on the scaffold of **N3**. In the first designed compound, **B1**, the recognition portion of **N3** was modified while both the recognition part and the warhead of **N3** (to a nitroalkene) were changed to generate a second compound, **B2** (Scheme 2).

The calculated free energy landscape for formation of the covalent enzyme-inhibitor intermediate indicate that the reaction, with all three compounds, proceeds in a stepwise manner: in the first step, Cys145 is activated by His41, forming the ion pair $\mathbf{E^{(+/-)}:I}$, followed in the second step by attack of the sulfur atom of Cys145 on the Cβ atom of the inhibitor and proton transfer from His41 to the Cα atom of the inhibitor, leading a stable covalent **E-I** intermediate. The rate-limiting step of the process, in all three cases, corresponds to the enzyme-inhibitor covalent bond formation, with an activation free energy of 11.2, 11.8 and 9.8 kcal·mol^{-1} for **N3**, **B1** and **B2**, respectively. The low activation free energy of the inhibition reaction with **N3** is in agreement with kinetic experiments,[12] while the values obtained with compound **B1** and **B2**, indicate that both are also reactive. Further, the lower activation energy for **B2** suggests that it would react faster with M^{pro}: this is a potential advantage in biological media in which the compounds have to compete with high concentration of the natural substrate. Within cells, covalent inhibitors must react with the target quickly, to avoid competing reactions with free bio-nucleophiles, such as glutathione, or with proteases (e.g. in the case of peptidyl compounds) that can reduce their active concentrations.[53] From the thermodynamic point of view, the exergonic process obtained with **N3** (reaction energy –17.9 kcal·mol^{-1}) is consistent with its experimentally observed stability (e.g. revealed by X-ray crystallographic structures).[12] The inactivation reactions of M^{pro} with **B1** and **B2** are also exergonic but are very different from each other (–27.9 and –11.4 kcal·mol^{-1}, respectively), suggesting that compound **B1** would be an irreversible inhibitor, but compound **B2** should present a more reversible character. Analysis of the QM-MM interaction energies between the different residues of the inhibitor and the residues located in the substrate-binding pockets of M^{pro} confirms the predictions assumed during the design of **B1** and **B2,** and the conclusions from geometrical analysis of the structures optimized at the DFT/MM level. In both cases, the interactions between the protein and the inhibitors are dominated by those in the P1:::S1 site. Finally, docking analysis carried out with the noncovalent enzyme:inhibitor reactant complex structures obtained from our QM/MM

structures support the proposal that **B1** and **B2** can bind M^{pro} in a reactive conformation in its active site.

In summary, our QM/MM study of the inhibition of M^{pro} by **N3** and two covalent (peptidyl) MA compounds, **B1** and **B2**, which we designed based on these simulations and medicinal chemistry experience, indicates that a lower alkylation barrier than **N3** can be obtained by modulating either the recognition portion or the warhead. Interactions between the recognition moiety and M^{pro} active site affect the chemical step because they dictate the pose of the inhibitor in the active site of the enzyme. Our results show that **B1** has a more irreversible character than **N**3 while **B2** is more reversible. This different behavior *in silico* suggest that both compounds should be tested and compared to **N3** as promising candidates as drug leads against COVID-19. Importantly, both designed compounds can be easily prepared through synthetic approaches inspired by published synthetic routes of similar compounds.

ASSOCIATED CONTENT

Electronic supplementary information (ESI) available:

Computational methods, FF parameters for inhibitors, detail of active site and QM-MM partitioning, M06-2X:AM1/MM FESs, list of average key inter-atomic distances in key states along the reaction path at AM1/MM and optimized at M06-2X/MM level, protein-substrate non-bonding interaction energies, per residue, cartesian coordinates of the QM sub-set of atoms and full structures (in PDB format) of the rate limiting TSs, E:I and E-I optimized at M06-2X/6-31+G(d,p)/MM level, and figure of inhibitors docked into the active site of SARS-CoV-2 M^{pro}.

AUTHOR INFORMATION

Corresponding Author

Katarzyna Świderek - Departament de Química Física i Analítica, Universitat Jaume I, 12071 Castelló, Spain; orcid.org/0000-0002-7528-1551; email: swiderek@uji.es

Vicent Moliner - Departament de Química Física i Analítica, Universitat Jaume I, 12071 Castelló, Spain; orcid.org/0000-0002-3665-3391; email: moliner@uji.es

Author Contributions

The study was designed by K.Ś., V.M., A.L. and A.J.M. The results were discussed and analyzed by all authors, who contributed to write the manuscript. K.A., N.S. and K.Ś. carried out the QM/MM calculations. A.L. carried out the docking calculations. All authors contributed to discussion and design of inhibitors. All authors have given approval to the final version of the manuscript.

ACKNOWLEDGMENT

This work was supported by the Spanish Ministerio de Ciencia, Innovación y Universidades (Grant PGC2018-094852-B-C21 and PID2019-107098RJ-I00), Generalitat Valenciana (Grant AICO/2019/195 and SEJI/2020/007) Universitat Jaume I (UJI·B2017-31, UJI·B2018-41, UJI-A2019-04 and SomUJIContraCovid crowdfunding campaign), KŚ thanks the Spanish Ministerio de Ciencia, Innovación y Universidades for a Juan de la Cierva – Incorporación (ref. IJCI-2016-27503) contract. K.A. thanks Universitat Jaume I (POSDOC-A/2018/30) and Generalitat Valenciana (APOSTD/2020/015) for post-doctoral contracts. NS thanks the

MINECO for doctoral FPI grant (BES-2016-078029). The authors thankfully acknowledge the computer resources at Pirineus and the technical support provided at Pirineus and by Barcelona Supercomputing Center (QSB-2020-2-0004), as well as the local computational resources of the Servei d'Informàtica of Universitat Jaume I. AJM thanks EPSRC for support (CCP-BioSim, grant number EP/M022609/1) and also the British Society for Antimicrobial Chemotherapy (grant number BSAC-COVID-30).

REFERENCES:

1. G. Zhu, C. Zhu, Y. Zhu and F. Sun, *Current Research in Microbial Sciences*, 2020, **1**, 53-61.
2. A. K. Ghosh, M. Brindisi, D. Shahabi, M. E. Chapman and A. D. Mesecar, *ChemMedChem*, 2020, **15**, 907-932.
3. R. T. Eastman, J. S. Roth, K. R. Brimacombe, A. Simeonov, M. Shen, S. Patnaik and M. D. Hall, *ACS Central Science*, 2020, **6**, 672-683.
4. T. Warren, R. Jordan, M. Lo, V. Soloveva, A. Ray, R. Bannister, R. Mackman, M. Perron, K. Stray, J. Feng, Y. Xu, J. Wells, K. Stuthman, L. Welch, E. Doerffler, L. Zhang, K. Chun, H. Hui, S. Neville, W. Lew, Y. Park, D. Babusis, R. Strickley, P. Wong, S. Swaminathan, W. Lee, D. Mayers, T. Cihlar and S. Bavari, *Open Forum Infectious Diseases*, 2015, **2**.
5. L. Zhang, D. Lin, X. Sun, U. Curth, C. Drosten, L. Sauerhering, S. Becker, K. Rox and R. Hilgenfeld, *Science*, 2020, **368**, 409-412.
6. J. H. Beigel, K. M. Tomashek, L. E. Dodd, A. K. Mehta, B. S. Zingman, A. C. Kalil, E. Hohmann, H. Y. Chu, A. Luetkemeyer, S. Kline, D. Lopez de Castilla, R. W. Finberg, K. Dierberg, V. Tapson, L. Hsieh, T. F. Patterson, R. Paredes, D. A. Sweeney, W. R. Short, G. Touloumi, D. C. Lye, N. Ohmagari, M.-d. Oh, G. M. Ruiz-Palacios, T. Benfield, G. Fätkenheuer, M. G. Kortepeter, R. L. Atmar, C. B. Creech, J. Lundgren, A. G. Babiker, S. Pett, J. D. Neaton, T. H. Burgess, T. Bonnett, M. Green, M. Makowski, A. Osinusi, S. Nayak and H. C. Lane, *New England Journal of Medicine*, 2020, DOI: 10.1056/NEJMoa2007764.
7. L. Lisi, P. M. Lacal, M. L. Barbaccia and G. Graziani, *Biochemical pharmacology*, 2020, DOI: 10.1016/j.bcp.2020.114169, 114169.
8. J. D. Norrie, *Lancet (London, England)*, 2020, **395**, 1525-1527.
9. L. Riva, S. Yuan, X. Yin, L. Martin-Sancho, N. Matsunaga, L. Pache, S. Burgstaller-Muehlbacher, P. D. De Jesus, P. Teriete, M. V. Hull, M. W. Chang, J. F.-W. Chan, J. Cao, V. K.-M. Poon, K. M. Herbert, K. Cheng, T.-T. H. Nguyen, A. Rubanov, Y. Pu, C. Nguyen, A. Choi, R. Rathnasinghe, M. Schotsaert, L. Miorin, M. Dejosez, T. P. Zwaka, K.-Y. Sit, L. Martinez-Sobrido, W.-C. Liu, K. M. White, M. E. Chapman, E. K. Lendy, R. J. Glynne, R. Albrecht, E. Ruppin, A. D. Mesecar, J. R. Johnson, C. Benner, R. Sun, P. G. Schultz, A. I. Su, A. García-Sastre, A. K. Chatterjee, K.-Y. Yuen and S. K. Chanda, *Nature*, 2020, DOI: 10.1038/s41586-020-2577-1.
10. T. Muramatsu, C. Takemoto, Y.-T. Kim, H. Wang, W. Nishii, T. Terada, M. Shirouzu and S. Yokoyama, *Proceedings of the National Academy of Sciences*, 2016, **113**, 12997-13002.
11. W. Dai, B. Zhang, X.-M. Jiang, H. Su, J. Li, Y. Zhao, X. Xie, Z. Jin, J. Peng, F. Liu, C. Li, Y. Li, F. Bai, H. Wang, X. Cheng, X. Cen, S. Hu, X. Yang, J. Wang, X. Liu, G. Xiao, H. Jiang, Z. Rao, L.-K. Zhang, Y. Xu, H. Yang and H. Liu, *Science*, 2020, **368**, 1331-1335.
12. Z. Jin, X. Du, Y. Xu, Y. Deng, M. Liu, Y. Zhao, B. Zhang, X. Li, L. Zhang, C. Peng, Y. Duan, J. Yu, L. Wang, K. Yang, F. Liu, R. Jiang, X. Yang, T. You, X. Liu, X. Yang, F. Bai, H. Liu, X. Liu, L. W. Guddat, W. Xu, G. Xiao, C. Qin, Z. Shi, H. Jiang, Z. Rao and H. Yang, *Nature*, 2020, **582**, 289-293.
13. J. Chodera, A. A. Lee, N. London and F. von Delft, *Nature Chemistry*, 2020, **12**, 581-581.
14. A. Latorre, T. Schirmeister, J. Kesselring, S. Jung, P. Johe, U. A. Hellmich, A. Heilos, B. Engels, R. L. Krauth-Siegel, N. Dirdjaja, L. Bou-Iserte, S. Rodriguez and F. V. Gonzalez, *ACS Medicinal Chemistry Letters*, 2016, **7**, 1073-1076.

15. P. A. Jackson, J. C. Widen, D. A. Harki and K. M. Brummond, *Journal of Medicinal Chemistry*, 2017, **60**, 839-885.
16. M. Gehringer and S. A. Laufer, 2019, **62**, 5673-5724.
17. A. Voice, G. Tresadern, H. van Vlijmen and A. Mulholland, *Journal of Chemical Information and Modeling*, 2019, **59**, 4220-4227.
18. R. A. Bauer, *Drug Discovery Today*, 2015, **20**, 1061-1073.
19. H. Yang, W. Xie, X. Xue, K. Yang, J. Ma, W. Liang, Q. Zhao, Z. Zhou, D. Pei, J. Ziebuhr, R. Hilgenfeld, K. Y. Yuen, L. Wong, G. Gao, S. Chen, Z. Chen, D. Ma, M. Bartlam and Z. Rao, *PLOS Biology*, 2005, **3**, e324.
20. J. W. Keillor and R. S. Brown, *Journal of the American Chemical Society*, 1992, **114**, 7983-7989.
21. K. Arafet, S. Ferrer and V. Moliner, *ACS Catalysis*, 2017, **7**, 1207-1215.
22. K. Świderek and V. Moliner, *Chemical Science*, 2020, DOI: 10.1039/D0SC02823A.
23. A. Lodola, M. Mor, J. Sirirak and A. J. Mulholland, *Biochemical Society Transactions*, 2009, **37**, 363-367.
24. K. Arafet, S. Ferrer and V. Moliner, *Biochemistry*, 2015, **54**, 3381-3391.
25. R. E. Amaro and A. J. Mulholland, *Nature Reviews Chemistry*, 2018, **2**, 0148.
26. D. Callegari, K. E. Ranaghan, C. J. Woods, R. Minari, M. Tiseo, M. Mor, A. J. Mulholland and A. Lodola, *Chemical Science*, 2018, **9**, 2740-2749.
27. N. Serrano-Aparicio, K. Świderek and V. Moliner, *European Journal of Medicinal Chemistry*, 2019, **164**, 399-407.
28. K. Arafet, F. V. González and V. Moliner, *Chemistry – A European Journal*, 2020, **26**, 2002-2012.
29. A. Lodola, D. Callegari, L. Scalvini, S. Rivara and M. Mor, *Methods in molecular biology (Clifton, N.J.)*, 2020, **2114**, 307-337.
30. L. Zhang, D. Lin, Y. Kusov, Y. Nian, Q. Ma, J. Wang, A. von Brunn, P. Leyssen, K. Lanko, J. Neyts, A. de Wilde, E. J. Snijder and H. Liu, 2020, **63**, 4562-4578.
31. S. A. Gillmor, C. S. Craik and R. J. Fletterick, *Protein Science*, 1997, **6**, 1603-1611.
32. E. Dunny, W. Doherty, P. Evans, J. P. G. Malthouse, D. Nolan and A. J. S. Knox, *Journal of Medicinal Chemistry*, 2013, **56**, 6638-6650.
33. S. Royo, S. Rodriguez, T. Schirmeister, J. Kesselring, M. Kaiser and F. V. Gonzalez, *ChemMedChem*, 2015, **10**, 1484-1487.
34. X. Zhai and T. D. Meek, *Biochemistry*, 2018, **57**, 3176-3190.
35. L. Zhu, S. George, M. F. Schmidt, S. I. Al-Gharabli, J. Rademann and R. Hilgenfeld, *Antiviral research*, 2011, **92**, 204-212.
36. P. S. Dragovich, T. J. Prins, R. Zhou, S. E. Webber, J. T. Marakovits, S. A. Fuhrman, A. K. Patick, D. A. Matthews, C. A. Lee, C. E. Ford, B. J. Burke, P. A. Rejto, T. F. Hendrickson, T. Tuntland, E. L. Brown, J. W. Meador, R. A. Ferre, J. E. V. Harr, M. B. Kosa and S. T. Worland, *Journal of Medicinal Chemistry*, 1999, **42**, 1213-1224.
37. G. M. Torrie and J. P. Valleau, *Journal of Computational Physics*, 1977, **23**, 187-199.
38. S. Kumar, D. Bouzida, R. H. Swendsen, P. A. Kollman and J. M. Rosenberg, *Journal of Computational Chemistry*, 1992, **13**, 1011-1021.
39. M. J. S. Dewar, E. G. Zoebisch, E. F. Healy and J. J. P. Stewart, *J. Am. Chem. Soc.*, 1985, **107**, 3902-3909.
40. Y. Zhao and D. G. Truhlar, *Theoretical Chemistry Accounts*, 2008, **120**, 215-241.
41. W. J. Hehre, L. Radom, P. v. R. Schleyer and J. A. Pople, *Ab Initio Molecular Orbital Theory*, New York, 1986.
42. M. J. Frisch, G. W. Trucks, H. B. Schlegel, G. E. Scuseria, M. A. Robb, J. R. Cheeseman, G. Scalmani, V. Barone, B. Mennucci, G. A. Petersson and H. C. Nakatsuji, M.; Li, X.; Hratchian, H. P.; Izmaylov, A. F.; Bloino, J.; Zheng, G.;

Sonnenberg, J. L.; Hada, M.; Ehara, M.; Toyota, K.; Fukuda, R.; Hasegawa, J.; Ishida, M.; Nakajima, T.; Honda, Y.; Kitao, O.; Nakai, H.; Vreven, T.; Montgomery, Jr., J. A.; Peralta, J. E.; Ogliaro, F.; Bearpark, M.; Heyd, J. J.; Brothers, E.; Kudin, K. N.; Staroverov, V. N.; Kobayashi, R.; Normand, J.; Raghavachari, K.; Rendell, A.; Burant, J. C.; Iyengar, S. S.; Tomasi, J.; Cossi, M.; Rega, N.; Millam, N. J.; Klene, M.; Knox, J. E.; Cross, J. B.; Bakken, V.; Adamo, C.; Jaramillo, J.; Gomperts, R.; Stratmann, R. E.; Yazyev, O.; Austin, A. J.; Cammi, R.; Pomelli, C.; Ochterski, J. W.; Martin, R. L.; Morokuma, K.; Zakrzewski, V. G.; Voth, G. A.; Salvador, P.; Dannenberg, J. J.; Dapprich, S.; Daniels, A. D.; Farkas, Ö.; Foresman, J. B.; Ortiz, J. V.; Cioslowski, J.; Fox, D. J. , *Gaussian 09 (Revision A.1)*, 2009.

43. K. Świderek, I. Tuñón, S. Martí and V. Moliner, *ACS Catalysis*, 2015, **5**, 1172-1185.
44. K. Świderek, I. Tuñón, V. Moliner and J. Bertran, *ACS Catalysis*, 2015, **5**, 2587-2595.
45. A. Krzemińska, V. Moliner and K. Świderek, *Journal of the American Chemical Society*, 2016, **138**, 16283-16298.
46. Y. Duan, C. Wu, S. Chowdhury, M. C. Lee, G. Xiong, W. Zhang, R. Yang, P. Cieplak, R. Luo, T. Lee, J. Caldwell, J. Wang and P. Kollman, *J Comput Chem*, 2003, **24**, 1999-2012.
47. W. L. Jorgensen, J. Chandrasekhar, J. D. Madura, R. W. Impey and M. L. Klein, *Journal of Chemical Physics*, 1983, **79**, 926-935.
48. M. J. Field, M. Albe, C. Bret, F. Proust-De Martin and A. Thomas, *J. Comp. Chem.*, 2000, **21**, 1088-1100.
49. R. A. Friesner, J. L. Banks, R. B. Murphy, T. A. Halgren, J. J. Klicic, D. T. Mainz, M. P. Repasky, E. H. Knoll, M. Shelley, J. K. Perry, D. E. Shaw, P. Francis and P. S. Shenkin, *Journal of Medicinal Chemistry*, 2004, **47**, 1739-1749.
50. J. R. A. Silva, L. Cianni, D. Araujo, P. H. J. Batista, D. de Vita, F. Rosini, A. Leitao, J. Lameira and C. A. Montanari, *Journal of chemical information and modeling*, 2020, **60**, 1666-1677.
51. A. Paasche, A. Zipper, S. Schäfer, J. Ziebuhr, T. Schirmeister and B. Engels, *Biochemistry*, 2014, **53**, 5930-5946.
52. C. A. Ramos-Guzmán, J. J. Ruiz-Pernía and I. Tuñón, 2020, DOI: 10.26434/chemrxiv.12895064.v1.
53. J. Singh, R. C. Petter, T. A. Baillie and A. Whitty, *Nature Reviews Drug Discovery*, 2011, **10**, 307-317.